Research

Trends, forecasting and adaptation strategies of climate change in the middle and west regions of Iraq

Waqed H. Hassan[1,2] · Basim K. Nile[2] · Zahraa K. Kadhim[2] · Karrar Mahdi[3] · Michel Riksen[3] · Rifqa F. Thiab[4]

© The Author(s) 2023   OPEN

Abstract

Climate change has placed considerable pressure on the residential environment, agricultural, and water supplies in different areas of the world, especially arid places such as Iraq. Iraq is one of the five most vulnerable countries in the world to climate change, where it has been encountering extremes heat waves during the most recent decades resulted in drought, desertification, and rivers dried up, which led to thousands of hectares to turn dry and yellow. This study aims to investigate the trends of climate change in the middle and western regions of Iraq and future expectations. The daily maximum temperature, minimum temperature, and precipitation are downscaled using the Long Ashton Research Station Weather Generator (LARS-WG) model. Five General Circulation Models (GCMs) from Coupled Model Intercomparison Project Phase 5 (CMIP5) are employed for three future periods: the near future (2021–2040), medium future (2051–2070), and far future (2081–2100), based on two scenarios of the Representative Concentration Pathways (RCP4.5 and RCP8.5) for four selected meteorological stations representing the study area. The outcomes of the calibration and validation of the model supported its skill and reliability to downscale precipitation and temperature time series for statistical indices (R^2, RMSE and MBE) ranging between (0.894–0.998), (0.1270–1.9274) and (− 0.6158 to 0.0008), respectively. The results showed that the average minimum and maximum annual temperatures will increase at all selected stations across the three future periods by between 0.94 and 4.98 °C by the end of the twenty-first century. Annual changes in precipitation tend generally towards increase for the study area by average (6.09–14.31%) for RCP4.5 and (11.25–20.97%) for RCP8.5 Compared to the historical data (1990–2020). These findings can contribute to become more acquainted with the effects of climate change on the environment and encourage managers and planners to come up with plans for mitigating and adapting to these effects. They can also serve as a guide for future management of water and agricultural resources in the study region.

Article Highlights

- The LARS-WG model effectively downscaled daily temperatures and precipitation in the middle and west regions of Iraq.
- A steady temperature increase in the current century in the study area between 0.94 and 4.98 °C.
- Future precipitation patterns vary, ranging from + 6.09 to + 14.31% for RCP4.5 and + 11.25 to + 20.97% for RCP8.5.

✉ Waqed H. Hassan, waqed.hammed@uowa.edu.iq; waaqidh@uokerbala.edu.iq; ✉ Karrar Mahdi, Karrar.mahdi@wur.nl; Michel Riksen, michel.riksen@wur.nl | [1]College of Engineering, University of Warith Al-Anbiyaa, Kerbala 56001, Iraq. [2]College of Engineering, University of Kerbala, Kerbala 56001, Iraq. [3]Soil Physics and Land Management Group, Wageningen University and Research, 6708 PB Wageningen, The Netherlands. [4]Al-Zahraa University for Women, Kerbala 56100, Iraq.

1 Introduction

The Middle East represents one of the area's most susceptible to the impacts of climate change as a result of the arid and semi-arid regions and its impact is evident in countries such as Turkey, Iran, Iraq, Kuwait, Saudi Arabia, Qatar, Sudan and Syria [1–4]. Climate change influence appears on the systems of the environment and humanity [5, 6], involving the risks associated with heat stress, storms and heavy rain, inland and flooding, dryness, scarce water supplies, and agriculture and food security [7, 8]. A consequence of the rising anthropogenic, greenhouse gas (GHG) emissions, which are mostly due to economic and population expansion. This has resulted in atmospheric quantities of carbon dioxide (CO_2), methane (CH_4), and nitrous oxide (N_2O) that have never been seen in centuries to millennia [9–11]. Their effects, together with those of other anthropogenic drivers [12].

The most straightforward and popular method of procedures for climate risk assessment is using the global climate models [13–15], which are powerful tools for modelling the three-dimensional climate system utilizing equations defining energy (first law of thermodynamics), momentum (Newton's second law of motion), conservation of mass (continuity equation), and water vapor (ideal gas law). Each equation is calculated for distinct layers of the atmosphere that are delineated by a regular grid at discrete locations on the Earth's surface, during predetermined periods of time [16, 17]. That used to study the future climate and its evolution by comparing the present and projected climatology in a Climate Model overlying the target region. However, due to their very coarse spatial resolution range from 100 to 300 km in horizontal resolution at grid cells [18–20], GCMs cannot be employed directly at a location, and their outputs are still vulnerable to biases [21]. Additionally, they have a limited ability to study regional-scale hydrological and physical atmospheric phenomena [22–24]. A popular technique for bridging the gap between coarse GCM output and values for climatic variables at a finer resolution is downscaling [25, 26]. Two widely recognized downscaling methods; dynamical downscaling (e.g., Regional Climate Models (RCMs)) and statistical downscaling (e.g., LARS-WS and SDSM) [27, 28]. Long Ashton Research Station Weather Generator (LARS-WG) and statistical downscaling models (SDSM), have emerged in recent years [29]. LARS-WG is based on a stochastic weather generator [30] while SDSM uses a regression-based approach [31].

According to the Fifth Assessment Report (AR5) of the Intergovernmental Panel on Climate Change (IPCC), Cumulative emissions of CO_2 largely determine global mean surface warming by the late twenty-first century and beyond [5]. To describe greenhouse gas (GHG) emissions in twenty-first century, used four Representative Concentration Pathways (RCPs). These scenarios are employed to evaluate the costs related to reducing emissions in line with specific concentration pathways. They include a stringent mitigation scenario (RCP2.6; scenario that aims to keep global warming likely below 2 °C above pre-industrial temperatures), two intermediate scenarios (RCP4.5 and RCP6.0), and one scenario with very high GHG emissions (RCP8.5). Projected to rise in global mean surface temperature under each of the evaluated emission scenarios throughout the twenty-first century between 0.3 and 4.8 and there will not be a uniform change in precipitation [5, 32]. And the predicts were compatibility with many studies conducted around the world such as; Europe [14], North America [33], Africa [34–37], and Asia [38–41]. In Turkey, an increase in temperature and a decrease in precipitation rates were projected during the twenty-first century [42], while in Iran, the temperature rise was with variable trends in precipitation [43].

Iraq is one of the countries in the Middle East that has been suffering greatly from climate change and has varied climates in each part of Iraq [44]. Iraq has been classified as the fifth-most vulnerable country to climate change due to both artificial and natural effects such as; a lack of vegetation and rise of total emissions of carbon dioxide as time passes as a result of increased crude oil production [45], methane emissions [46], and other greenhouse gases are increasing dramatically [47]. Where Iraq was listed in the top five countries in flaring activities for petroleum industry [48] because Iraq's economy relies heavily on oil revenues [49]. Researchers [50–53] studied the effect of climate change in the southern parts of Iraq, and the results showed that that temperatures will rise during the twenty-first century, and the amounts of precipitation will vary in changing tends while the precipitation trends may decrease in the northern and eastern regions of the country, and this is what the studies conducted by Saeed et al. [54], and Osman et al. [55] show. Iraq is facing severe water scarcity due to dams built by Syria, Iran, and Turkey on the Tigris and Euphrates Rivers [56]. 22 dams were built as part of the Southeastern Anatolia Project [57], while Syria constructed three along the Euphrates River. In addition to the foregoing, Iran recently redirected all perennial valleys within Iran that went into Iraq [58]. These dams have led to

decreased river flow and water quality, land degradation, desertification, and an increase in climate change [59, 60]. Additionally, poor water management strategies, such as flood irrigation and outdated agricultural practices, further exacerbate the scarcity [61]. The agricultural sector consumes 95% of available freshwater, resulting in high water consumption [62, 63].

This study was undertaken with the objective to forecast minimum, maximum temperatures and precipitation for the in middle and western areas of Iraq for the three chosen time periods of 2021–2040, 2051–2070, and 2081–2100. This will help to investigate the effects of climate change on water resources, on agricultural crop production, and on livelihoods in these areas. These areas have extensive deserts and are at risk for dust storms, high temperatures, and greater rates of evaporation. Here, climate change is having a major impact on the Tigris and Euphrates rivers, leading to changes in annual stream flow volumes with decreased water income from Turkey and Iran to the two rivers [64]. Variation of rainfall amounts, resulting in long drought periods [50], can also cause changes in land vegetative cover. Increased temperatures also cause changes in physical and chemical characteristics of the soil, and leading to loss of soil moisture and vegetation cover in Iraq's arable and non-arable lands [65].

In this study, the LARS-WG model version 6.0 was utilized to downscale GCMs output. This version incorporates climate projections from Phase 5 of the Coupled Model Intercomparison Project (CMIP5) ensemble used in the IPCC Fifth Assessment Report (AR5). Five models were implemented under two scenarios of Representative Concentration Pathways RCP4.5 and RCP8.5.

2 Material and methods

2.1 Study area

The study area is located in the middle and western regions of Iraq, covering 166,098 km². It is located between latitudes (29° 53′ 5″–35° 9′ 25″) N and longitudes (38° 45′ 12″–44° 44′ 4″) E and includes three cities: Kerbala, Najaf, and Anbar, whose locations are shown in Fig. 1. The study area has dry and extreme summer temperatures during (July and August) and a cool to cold winter, with the average annual maximum and minimum temperatures are 30 ℃ and 16 ℃, respectively. The annual mean rainfall between 81 and 123 mm. The study area is the most important groundwater reservoir in Iraq [66] and contains large agricultural areas with large proportion of the study area is a desert extending to the west in Kerbala, Najaf and Anbar.

Table 1 shows information of the 4 meteorological stations of which the data was used in this study. The validation and calibration process of the weather generator model used historical data for daily precipitation, maximum, and minimum temperatures over 30 years (1990–2020). These data obtained from the international

Fig. 1 Study area and the chosen meteorological stations positions (ArcGIS (ArcMap) software version10.8 was used to generate this Figure. (URL link: https://desktop.arcgis.com/en/arcmap/latest/get-started/setup/arcgis-desktop-system-requirements.htm)
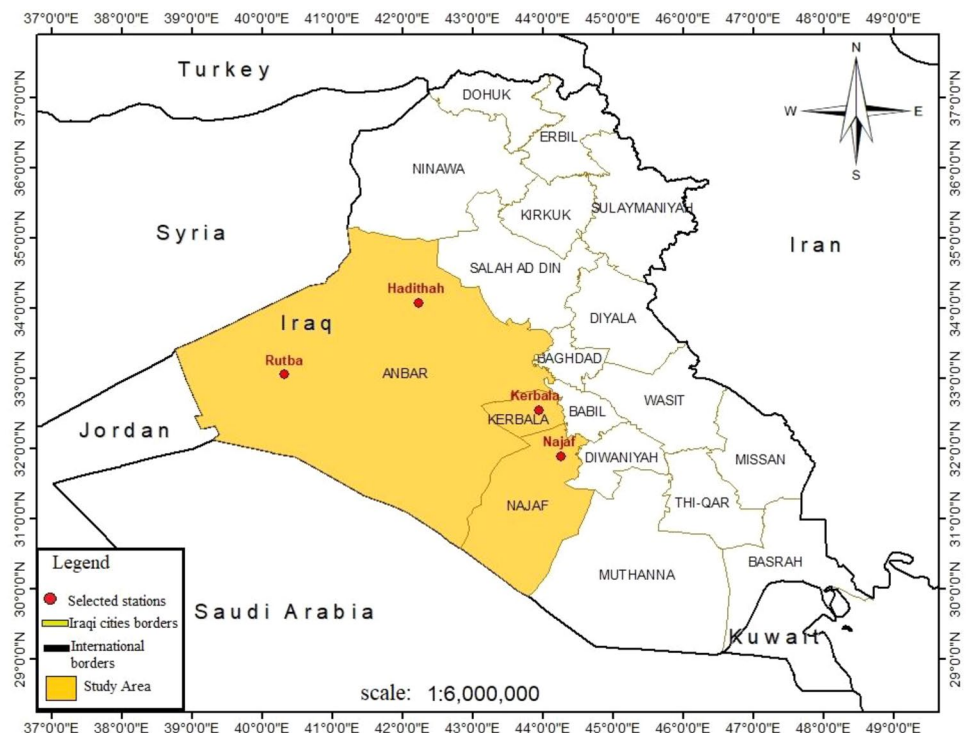
Table 1 Location information for the four selected stations in the study area

Station	City	Latitude	Longitude	Elevation (m)	Period of records
Kerbala	Kerbala	32° 34′ 12″ N	44° 3′ 0″ E	29	1990–2020
Najaf	Najaf	31° 57′ 0″ N	44° 19′ 12″ E	53	1990–2020
Hadithah	Anbar	34° 7′ 48″ N	42° 21′ 0″ E	108	1990–2020
Rutba	Anbar	33° 1′ 48″ N	40° 16′ 48″ E	222	1990–2020

meteorological database for Climate Forecast System Reanalysis (CFSR) for period January 1990 to December 2014 (https://swat.tamu.edu/data/cfsr). The addition daily climatic data from 2015 to 2020 is taken from the projection of Worldwide Energy Resources (POWER) project. The POWER project data was obtained from the National Aeronautics and Space Administration (NASA) Research (https://power.larc.nasa.gov/).

2.2 LARS-WG model

There are two technologies to downscaling of Global Climate Model (GCMs), dynamical and statistical. Dynamical downscaling requires advanced devices and equipment and types of computers with high specifications, which are not available in many countries in the world, including Iraq and the region. Because of this, statistical methods are resorted to downscaling, which do not require high computing capabilities compared to dynamic downscaling. However, there is uncertainty in using statistical downscaling, and due to the lack of models specific to the study area, more models are used to reduce uncertainty.

Long Ashton Research Station Weather Generator (LARS-WG) is the stochastic weather generator tool, which is a type of statistical downscaling. LARS-WG has been widely utilized in downscaling studies across the world [36] because of the LARS-WG software is basic but flexible and computationally efficient and utilized to simulate weather data for both present and upcoming climatic events from 2011 to 2100 based on historical data at a single site supplied by GCMs [67]. These data are daily time-series for a number of climate variables, including precipitation (mm), maximum and lowest temperatures (°C), and solar radiation (MJ m^{-2} day^{-1}) [30], but not take into consideration the effect of cover land. In situations where solar radiation data is unavailable at a specific location, sunshine hours can be used instead, and the weather generator automatically converts these hours to solar radiation by applying an algorithm. The primary variable is precipitation, and the other three variables on a given day are determined by whether the day is wet or dry. Precipitation occurrence is simulated using distributions of the length of continuous sequences, or series, of wet and dry days [68]. The semi-empirical distribution (SED) is a method used by LARS-WG to approximate the probability

distributions of dry and wet series, daily precipitation, minimum and maximum temperatures, and solar radiation. Equation (1) was used to determine the value of the climate variable v_i that corresponds to the probability P_i for each climate variable v.

$$v_i = min\{v : P(v_{obs} \leq v) \geq P_i\}; \quad i = 0, \dots, n \quad (1)$$

where $P(v_{obs} \leq v)$ represents the probability depending on v_{obs}, the observed data. Two values, P_0 and P_n, remain constant as $P_0 = 0$ and $P_n = 1$, respectively, with according values for $v_0 = min\ v_{obs}$ and $v_n = max\ v_{obs}$, depending upon the climatic variable. Some P_i is allocated approximately zero for the lowest value, while approximately to 1 for the highest value, in order to correctly imitate the extreme values of a climatic variable. The other P_i values are then evenly spread over the probability range. Three values that are near to 1 are chosen for precipitation: $P_{n-1} = 0.999$, $P_{n-2} = 0.995$, and $P_{n-3} = 0.985$. These values enable more accurate calculation of exceptionally high daily precipitation occurrences with extremely low probability. Due to the probability of very low daily precipitation (< 1 mm) being typically relatively high and such low precipitation having very little impact on the output of a process-based impact model, we only use two values, $v_1 = 0.5$ mm and $v_2 = 1$ mm, to approximate precipitation within the range (0,1). The corresponding probabilities are calculated as $P_i = P(v_{obs} \leq v_i); i = 1, 2$. Two values close to 1 are used in SEDs for wet and dry series, $P_{n-1} = 0.99$ and $P_{n-2} = 0.98$, to account for excessively long dry and wet series. Two values near 0 and two values near 1 are used to accommodate for exceptionally high and low temperatures for maximum and minimum temperatures, respectively, i.e., $P_2 = 0.01$, $P_3 = 0.02$, $P_{n-1} = 0.99$, and $P_{n-2} = 0.98$. Due to physical constraints, all P_i values (0 < i < n) for radiation have an even distribution between minimum and maximum values. This study utilized the latest version, 6.0 LARS-WG, to simulate future climate change for three periods; 2021–2040, 2051–2070 and 2081–2100) for the baseline period 1990–2020.

2.3 Global Climate Model (GCMs)

Global Climate Model (GCMs) are commonly used to simulate the current climate and forecast the future climate.

There are nineteen climate models of GCMs included in LARS-WG version 6, which incorporates climate projection s from CMIP5 used in the Intergovernmental Panel on Climate Change (IPCC) Fifth Assessment Report (AR5) [5].

By choosing the appropriate number of models that are appropriate and according to the study area and it is crucial to take in mind that all GCM and RCP combinations should be considered equally plausible with the assessment of the uncertainty of the future projection s of the models through validation in comparison with the baseline data for the selected locations [69]. On the basis of earlier research conducted in Iraq to assess the most suitable models to be applied in the forecasting of future climate change. The five models and 2 Representative Concentration Pathways (RCP), intermediate stabilization scenario RCP4.5 and high emission scenario RCP8.5 (illustrated in Table 2) to project changes in maximum, minimum temperatures and precipitation in the current research.

2.4 Data available and outline of the modeling procedures with LARS-WG

Two data sets of observed weather required to available for each site in designing weather generators to produce synthetic weather data. The first consisted of daily values of minimum and maximum temperature, precipitation and radiation or sunshine hours over relatively long periods of between 20 and 30 years is recommended. The second data set is a (*.st) file containing details about the position; name of station, longitude, latitude, and altitude and CO_2. After prepared the two files, start the steps of the modeling procedures using LARS-WG [30].

1. Analysis: The observed daily weather at a site is analyzed (model calibration) to calculate site parameters. The data is saved in three files: a (*.wgx) file that contains the site parameters, a (*.stx) file that contains some additional statistics, and a (*.tst) file that contains results of LARS-WG statistical tests.
2. Generator: To generate synthetic daily weather (a baseline scenario) that is statistically comparable (model

validation) to observed weather at a location, the site parameter file (*.wgx) file is used, then can create a local-scale future scenario that matches to the forecast future climate by applying baseline site characteristics for climatic changes generated from a global or local climate model.

2.5 Model performance indices

LARS-WG computes a (*.tst) file with results of statistical tests comparing synthetic and observed weather when the site parameters are computed during calibration and validation. Statistical tests include the t-test to compare monthly means (12 tests) computed using Eq. (2). And the f-test to compare monthly standard deviations, shown in Eq. (3). The Kolmogorov–Smirnov (K-S) test compares probability distributions of daily factors every month in each location (12 tests) and for the seasonal distribution of the length of dry and wet series, the KS-test was used (4 tests), shown in Eq. (4). In order to determine how likely it is that the data came about by chance, presuming the null hypothesis was correct, we computed a *p* value for each test. If the *p* value is exceedingly low, less than 0.01 or 0.05, the generated climate is unable to be similar to the observed climate. With the value of 0.05, a common significant level used in statistical tests [68]. A perfect fit with a value of ($p = 1$), a very good fit ($0.7 \leq P < 1$) and good ft has a *p* value ($0.4 \leq P < 0.7$), while a poor ft is a ($P < 0.4$).

$$t = \frac{\overline{x}_1 - \overline{x}_2}{\sqrt{\frac{S_1^2}{n_1 - 1} - \frac{S_2^2}{n_2 - 1}}} \qquad (2)$$

where $\overline{x}_1$ and $\overline{x}_2$ indicate the means of the both observed and generated datasets. S_1^2 and S_2^2 are the standard deviations of both datasets, and $n_1 - 1$ and $n_2 - 1$ are the sizes of the two data sets.

$$f = \frac{S_1^2}{S_2^2} \qquad (3)$$

Table 2 Five Selected GCMs from IPCC AR5 included in LARS-WG 6 and with RCP4.5 and RCP8.5 scenarios

No.	GCM	Research center	Spatial resolution	RCP
1	NorESM1-M	Norwegian Climate Center, Norway	2.0° × 2.0°	4.5, 8.5
2	CanESM2	Canadian Centre for Climate Modeling and Analysis, Canada	2.8° × 2.8°	4.5, 8.5
3	MIROC5	Atmosphere and Ocean Research Institute (The University of Tokyo), National Institute for Environmental Studies, and Japan Agency for Marine-Earth Science and Technology, Japan	1.4° × 1.4°	4.5, 8.5
4	HadGEM2-ES	Met Office Hadley Center, United Kingdom	1.2° × 1.8°	4.5, 8.5
5	CSIRO-Mk3.6	Commonwealth Scientific and Industrial Research Organization, Australia	1.8° × 1.8°	4.5, 8.5

where S_1^2 is variance of the observed data and S_2^2 is variance of the generated data.

$$D = |(Fn_1(x) - Fn_2(x))| \qquad (4)$$

where n_1= observed data, n_2= generated data. Additional statistical criteria used to assess the performance of LARS-WG model, are the coefficient of determination (R^2), root mean square error (*RMSE*), and mean bias error (*MBE*) computed using Eqs. (5), (6) and (7), respectively. R^2 has a range from 0 to 1, and the optimum value is $R^2 = 1$.

$$R = \frac{\sum_i^n (x - \overline{x})(y - \overline{y})}{\sqrt{\sum_i^n (x - \overline{x})^2 \sum_i^n (y - \overline{y})^2}}; \quad i = 1, \ldots, \ldots, n \qquad (5)$$

R^2, which is the square of this correlation coefficient. Where; x, y refer to observed and generated datasets, $\overline{x}$, $\overline{y}$ refer to the mean observed and generated datasets. *RMSE* is an error-index type of model evaluation statistic. The model performs better the closest this value is to zero, shown in Eq. (6)

$$RMSE = \sqrt{\frac{\sum_i^n (P_i - O_i)^2}{n}}; \quad i = 1, \ldots, \ldots, n \qquad (6)$$

MBE represents the error in estimation of modeling. It might be a positive or negative in value, and zero is the optimum value, shown in Eq. (7)

$$MBE = \frac{\sum_i^n (P_i - O_i)}{n}; \quad i = 1, \ldots, \ldots, n \qquad (7)$$

where P_i represents the projected daily value for climate variables, and O_i represents the observed daily value and n is the total number of data used.

For calibration and validation of the model, daily time series of precipitation, maximum and minimum temperatures from 1990 to 2020 selected as the baseline years, for the four weather stations in the study area. When the site parameters are computed, LARS-WG computes a (*.tst) file that include results of statistical tests comparing synthetic and observed weather.

3 Results

3.1 Calibration and validation of LARS-WG model

The calibration and validation of the model results of the model shown in Table 3 (the seasonal observed data) and Table 4 (the simulated daily rainfall for every month). The number of tests conducted is indicated in both tables by the letter N. From the results in Tables 3 and 4, it can be

Table 3 K–S test for distributions of the seasonal wet and dry series

Season	Wet/dry	N	K–S	P value	Assessment
Kerbala station					
DJF	Wet	12	0.03	1	Perfect
DJF	Dry	12	0.038	1	Perfect
MAM	Wet	12	0.069	1	Perfect
MAM	Dry	12	0.112	0.997	Very good
JJA	Wet	12	0.044	1	Perfect
JJA	Dry	12	0.131	0.982	Very good
SON	Wet	12	0.069	1	Perfect
SON	Dry	12	0.084	1	Perfect
Najaf station					
DJF	Wet	12	0.062	1	Perfect
DJF	Dry	12	0.042	1	Perfect
MAM	Wet	12	0.057	1	Perfect
MAM	Dry	12	0.244	0.443	Good
JJA	Wet	12	0	1	Perfect
JJA	Dry	12	0.174	0.842	Very good
SON	Wet	12	0.053	1	Perfect
SON	Dry	12	0.044	1	Perfect
Hadithah station					
DJF	Wet	12	0.064	1	Perfect
DJF	Dry	12	0.035	1	Perfect
MAM	Wet	12	0.07	1	Perfect
MAM	Dry	12	0.096	1	Perfect
JJA	Wet	12	0.13	0.984	Very good
JJA	Dry	12	0.174	0.842	Very good
SON	Wet	12	0.07	1	Perfect
SON	Dry	12	0.091	1	Perfect
Rutba station					
DJF	Wet	12	0.057	1	Perfect
DJF	Dry	12	0.061	1	Perfect
MAM	Wet	12	0.061	1	Perfect
MAM	Dry	12	0.103	0.999	Very good
JJA	Wet	12	0.836	0	Poor
JJA	Dry	12	0.223	0.56	Good
SON	Wet	12	0.076	1	Perfect
SON	Dry	12	0.047	1	Perfect

concluded that the LARS-WG model for the four stations is well capable to simulate the weather for all stations in wet and dry series distributions. During winter (DJF) and autumn (SON), the results showed a perfect fit. In the summer (JJA), the model gave a very good to perfect fit expected the wet series of Rutba station is poor, and the evaluation spring season (MAM) gave a good to perfect fit. The results of the evaluations in Table 4 show that the performance of the LARS-WG when simulating daily rainfall distributions, varied from very good to perfect fit in all months except the summer months showed a poor fit. Since there is little to no rainfall during those months, the

Table 4 K–S-test for distributions of daily rainfall

Month	N	K–S	P value	Assessment
Kerbala station				
J	12	0.047	1	Perfect
F	12	0.062	1	Perfect
M	12	0.072	1	Perfect
A	12	0.096	1	Perfect
M	12	0.076	1	Perfect
J	12	0.479	0.006	Poor
J	12	0.522	0.002	Poor
A	No precipitation			
S	12	0.261	0.359	Poor
O	12	0.079	1	Perfect
N	12	0.059	1	Perfect
D	12	0.062	1	Perfect
Najaf station				
J	12	0.086	1	Perfect
F	12	0.063	1	Perfect
M	12	0.083	1	Perfect
A	12	0.077	1	Perfect
M	12	0.075	1	Perfect
J	12	0.479	0.006	Poor
J	12	0.652	0	Poor
A	12	0.609	0	Poor
S	12	0.348	0.096	Poor
O	12	0.093	1	Perfect
N	12	0.06	1	Perfect
D	12	0.052	1	Perfect
Hadithah station				
J	12	0.019	1	Perfect
F	12	0.032	1	Perfect
M	12	0.135	0.976	Very good
A	12	0.034	1	Perfect
M	12	0.027	1	Perfect
J	12	0.348	0.096	Poor
J	12	0.565	0.001	Poor
A	No precipitation			
S	12	0.435	0.017	Poor
O	12	0.041	1	Perfect
N	12	0.048	1	Perfect
D	12	0.132	0.981	Very good
Rutba station				
J	12	0.081	1	Perfect
F	12	0.03	1	Perfect
M	12	0.066	1	Perfect
A	12	0.043	1	Perfect
M	12	0.055	1	Perfect
J	12	0.522	0.002	Poor
J	12	0.479	0.006	Poor
A	12	0.218	0.589	Good
S	12	0.435	0.017	Poor
O	12	0.045	1	Perfect

Table 4 (continued)

Month	N	K–S	P value	Assessment
N	12	0.054	1	Perfect
D	12	0.025	1	Perfect

simulation of rainfall patterns performs poorly. Overall, it can be concluded that the model's simulations of the daily rainfall showed a good fit.

The statistics generated from the simulated and corresponding ones calculated from the observed database have been compared in order to raise trust in LARS-WG's capacity to generate maximum temperature, minimum temperature, and precipitation in the future. Depicts charts of the monthly mean and standard deviation generated data from historical and simulated in the study area, are shown in Fig. 2. Figure 2 showed the monthly mean and standard deviation, which modeled by LARS-WG for precipitation, minimum and maximum temperatures. Bearing in mind that previous research indicated that obtaining high degree of concordance between observed and computed values of precipitation is more complex and challenging than temperature because of intermediary processes including humidity, cloud cover.

Table 5 and Fig. 3 shows the values of the root-mean-square error (RMSE), mean bias error (MBE) and coefficient of determination (R^2) between the observed data and simulated data for the mean monthly values of temperatures and precipitation for the selected stations. It can be seen from Fig. 3, the R^2 for the mean monthly maximum temperature, minimum temperature and precipitation had strong lines relationship between observed and simulation data, ranging between (0.894–0.998) for all three climate variables. The values for the root mean square error (RMSE) and mean bias error (MBE) ranged between (0.1270–1.9274) and (-0.6158 to 0.0008), respectively, for the climate variables. Overall, the model performs can be considered reasonably good when generating temperatures and precipitation, allowing it will be used to forecast the weather in the future.

3.2 Projection of future temperatures

After calibration and verification of LARS-WG model, the weather generator model developed for each selected station (Kerbala, Najaf, Hadithah and Rutba) under study area in Iraq was used to project future daily for precipitation, maximum temperatures and minimum temperature for period from 2021 to 2100 (the end of the twenty-first century). In this study, the future period was divided into three periods: 2021–2040 (near future), 2051–2070 (medium future) and 2081–2100 (far future). Five GCMs
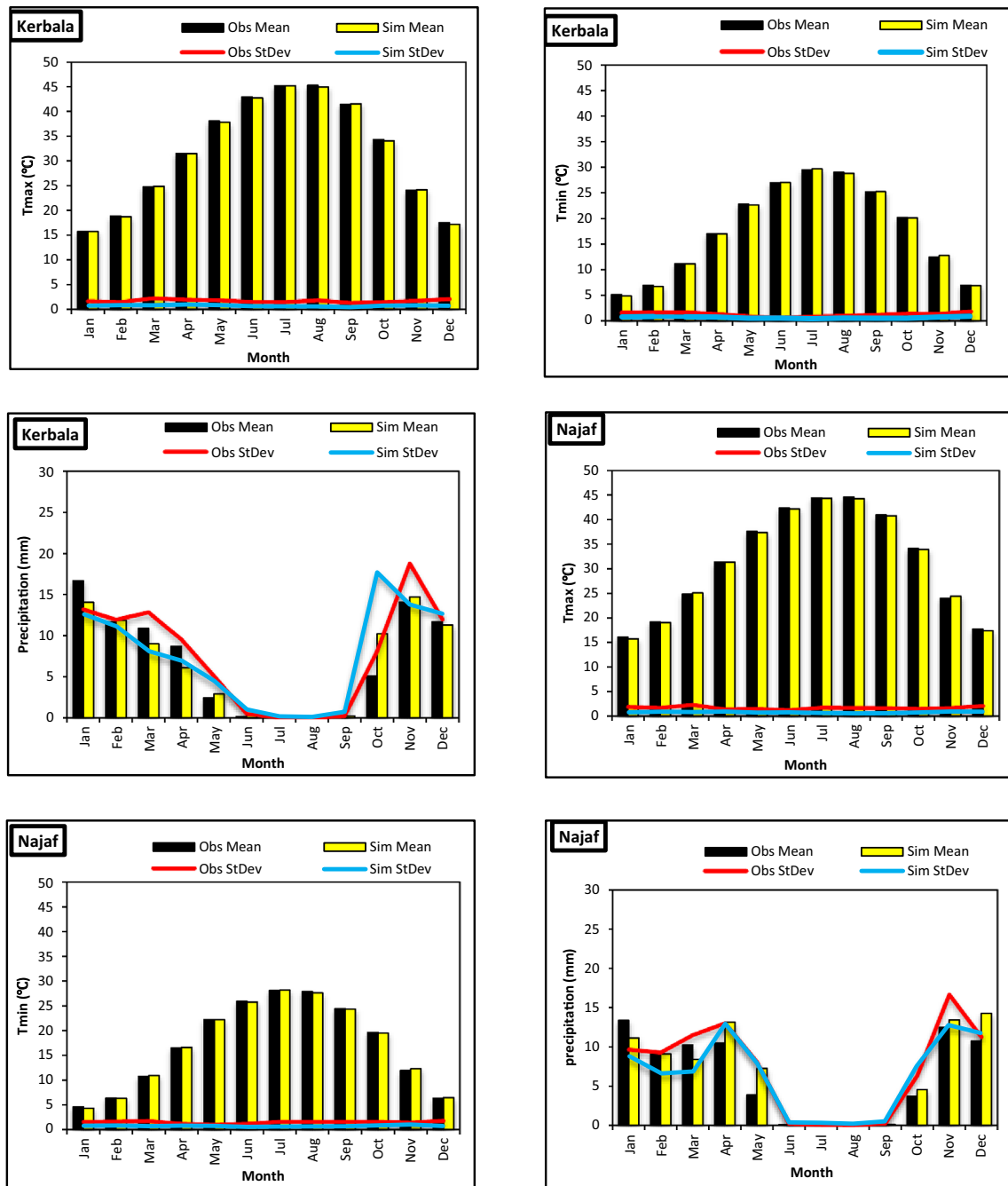
Fig. 2 Comparison of observed and simulated monthly mean and standard deviation for maximum, minimum temperatures and precipitation

(NorESM1-M, CanESM2, CSIRO-MK3.6.0, HadGEM2-ES and MIROC5) were employed with scenarios RCP4.5 and RCP8.5. The results of the future temperatures can be seen in Figs. 4 and 5.

Figure 4 shows the average monthly temperatures of observed (1990–2020) and average values of five GCMs models predicted for three periods (2021–2040, 2051–2070, and 2081–2100) under scenarios RCP4.5 and

RCP8.5. The charts appear steady growth of Tmax and Tmin with the time for all stations under each scenario, in which lest values of T max and T min recorded at the period (1990–2020) and the high values at period (2081–2100). January has the lowest averages of temperatures, while July and august have the highest average temperature in all four stations. Kerbala will record the highest value of maximum predicted temperatures in the far future
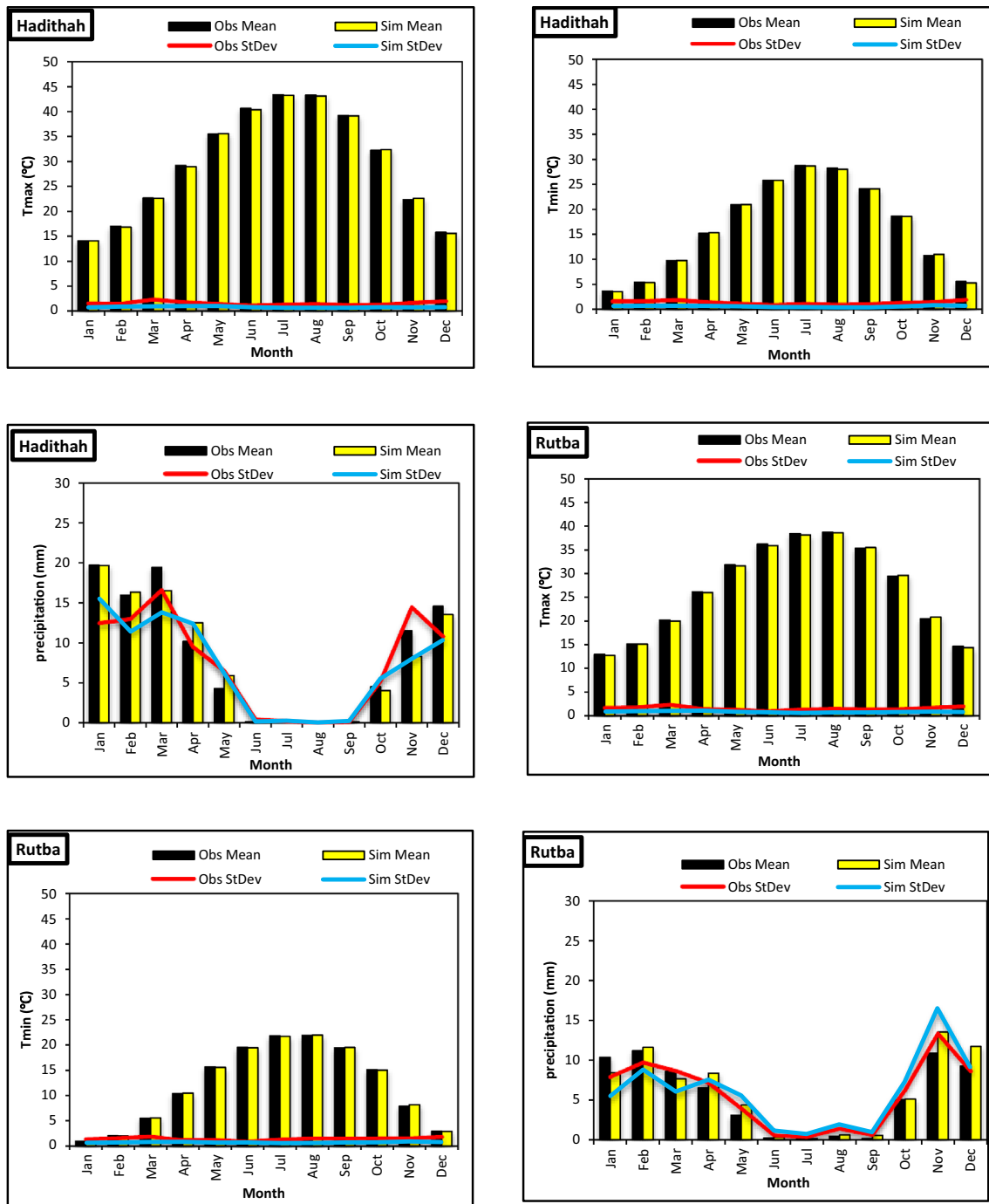
Fig. 2 (continued)

(2081–2100) under scenario RCP8.5, reaching a peak of 51.16 °C in August.

Figure 5 shows the annual temperatures differences between three periods that predicted by the selected five GCMs models and observed period. The charts appear the average annual maximum temperatures will be risen during the twenty-first century for all four stations; Kerbala, Najaf, Hadithah and Rutba under each

scenario (RCP4.5 and RCP8.5) for the five GCMs models by about (0.62–3.25) °C under RCP4.5, (0.83–5.91) °C under RCP 8.5 for Kerbala station, (0.68–3.3) °C under RCP4.5, (0.86–5.95) °C under RCP8.5 for Najaf station. For a Hadithah and Rutba stations, the increase will be between (0.63–3.29) °C and (0.57–3.29) °C under RCP4.5, (0.86–5.81) °C and (0.8–5.72) °C under RCP8.5. The least difference of maximum temperature was predicted by

Table 5 Statistical indexes of calibration and validation model for Tmax, Tmin and Precipitation

Station	Climate variable	R^2	RMSE	MBE
Kerbala	Tmax	0.9996	0.198305	− 0.10083
	Tmin	0.9997	0.179884	− 0.0275
	Precipitation	0.8948	1.927446	− 0.06333
Najaf	Tmax	0.9995	0.248831	− 0.105
	Tmin	0.9996	0.186503	− 0.00167
	Precipitation	0.8961	1.852977	− 0.61583
Hadithah	Tmax	0.9998	0.170318	− 0.0625
	Tmin	0.9998	0.14151	− 0.03583
	Precipitation	0.9668	1.537406	− 0.28167
Rutba	Tmax	0.9995	0.223644	− 0.08667
	Tmin	0.9997	0.126984	0.000833
	Precipitation	0.9273	1.389862	− 0.55833

CSIRO-MK3.6.0 model under RCP4.5 and NorESM1-M model add to it under RCP8.5 while HadGEM2-ES model have the highest difference of temperatures under each scenario RCP4.5 and RCP8.5. The highest of difference Tmax was at Najaf station, about 5.95 °C under RCP8.5 for HadGEM2-ES model. The average annual increases in minimum and maximum temperatures for all four stations are shown in Fig. 6. The result of the RCP 8.5 showed the biggest difference in temperatures range (1.07–4.9) °C for Tmax and (1.13–5.07) °C for Tmin while RCP 4.5 showed the smallest difference, with (0.93–2.64) °C for Tmax and (0.95–2.52) °C for Tmin. Overall, the average increasing of predicted temperature during twenty-first century is between 0.94 and 4.98 °C for all four selected stations (Fig. 7). Figure 7a and b show the Spatial distribution of the projected changes in average temperature relative to the reference baseline historical data (1990–2020) and the projected average temperatures under RCP 4.5 and RCP 8.5 scenarios for future periods (2021–2100). These results are consistent with previous studies by Salman et al. [70], Pirttioja et al. [71], Hassan and Hashim [72].

3.3 Projection of future precipitation

The results show a clear temporal and spatial variation in the amounts of precipitation, its intensity, directions, and timing in the study area. This is due to the lack of continuity of precipitation during the year and its lack and scarcity in the summer months, it is difficult to obtain a stable trend of precipitation in the study area. In general, the most common characteristic is that most of the rain tends towards a fluctuate increase in its amounts annually and monthly during the rainy months (from October to May), except some months that will witness a decrease from the monitored amounts, such as December in Kerbala,

February in Rutba, (February and January) in Najaf, and (April and October with a very few drops) in Hadithah station, as shown in Fig. 8. The charts show, a variation in precipitation during the near, medium and long future periods for each station.

Figure 9 shows the seasonal difference in precipitation for the five models for three periods; The near future (2021–2040), the medium future (2051–2070), and the distant future (2081–2100). The results show that the highest increase in precipitation amounts, for each scenario RCP4.5 and RCP8.5, was predicted by the CanESM2 model. Where the highest amount of precipitation increased from the average by 12.2 mm in the Hadithah station of the model CanESM2 under the scenario RCP8.5 in winter (DJF) for the period 2081–2100. While the least estimated rainfall decrease is predicted by the model MIROC5 under a scenario RCP8.5 in winter (DJF) and for a period 2081–2100 in Kerbala station about 5.62 mm. The percentage of annual increase in precipitation in the rainy months begin of October to May for average of the four stations (Kerbala, Najaf, Hadithah and Rutba) and according to future periods from 2021 until the end of the twenty-first century is shown in Fig. 10. Where the figure shows that the annual percentage increase in precipitation over the observed is variable for each period and under each of the scenarios (RCP4.5 and RCP8.5). It ranges between (6.09–14.31%) for RCP4.5 and (11.25–20.97%) for RCP8.5. These results are consistent with previous research by Hassan [73].

4 Discussion

According to the results of the statistical indexes used, the LARS-WG model can be considered reasonably good for generating projected temperatures and precipitation in the study area (the middle and western regions of Iraq), allowing it to be used to forecast the weather in the future.

For the temperatures, the results indicate an increase projected for all four selected field stations of an average of 0.94–4.98 °C for the future period of the twenty-first century. This wide variation in the projected increase is due to the different emission scenarios used in the study. On the other side, the uncertainty of the downscaling process can be a direct effect of the projected results. In general, the results are consistent with many previous studies conducted by researchers in Iraq, such as researchers [50, 52, 72, 74]. Moreover, the results of these studies and the current study show that the general trend of projected increasing temperatures in Iraq tends towards an increase in rates that vary according to location. Where the increase is to a lesser degree in the northern regions, it increases more towards the central and western regions and reaches its peak in the southern regions of Iraq.
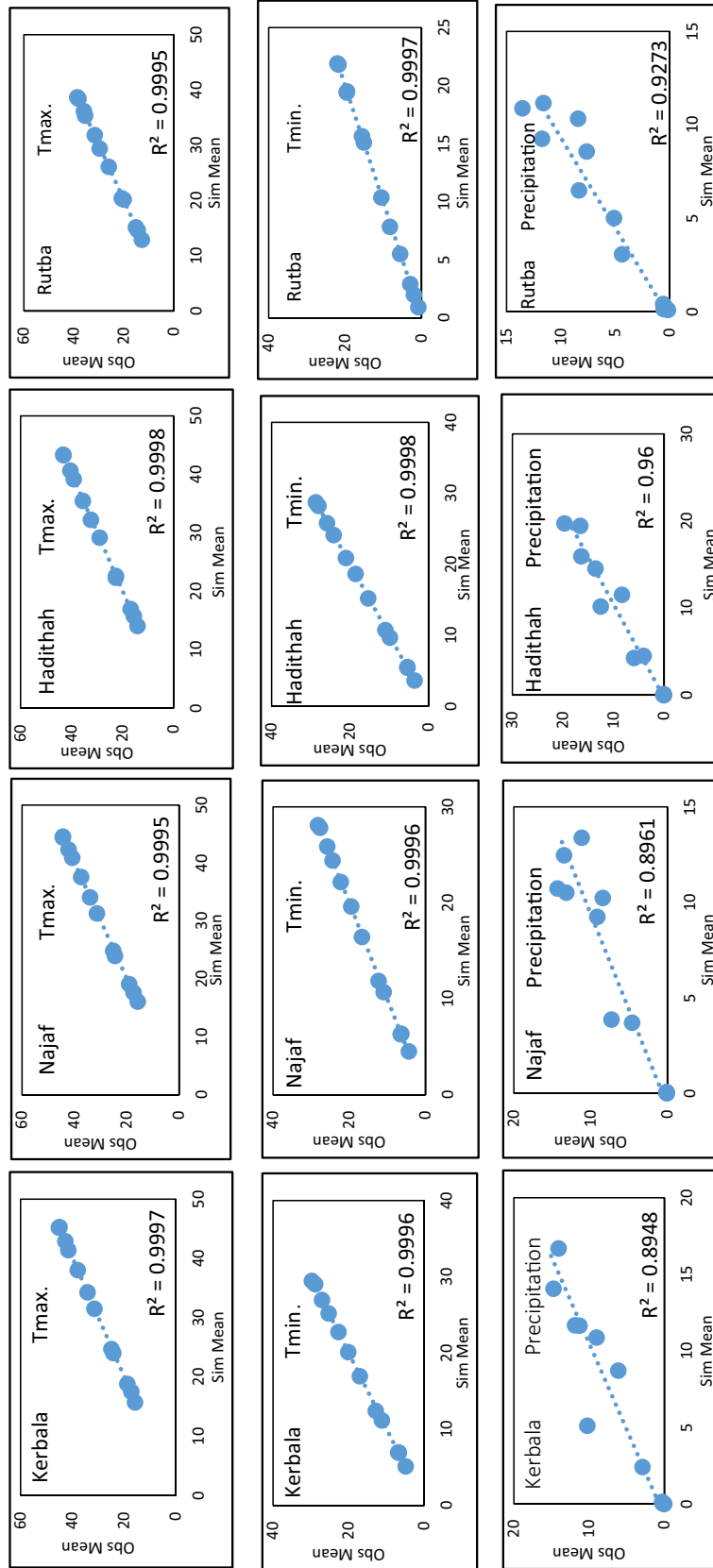
Fig. 3 Validation models and the coefficient of determination (R^2) for Tmax, T min, and Precipitation for all selected stations
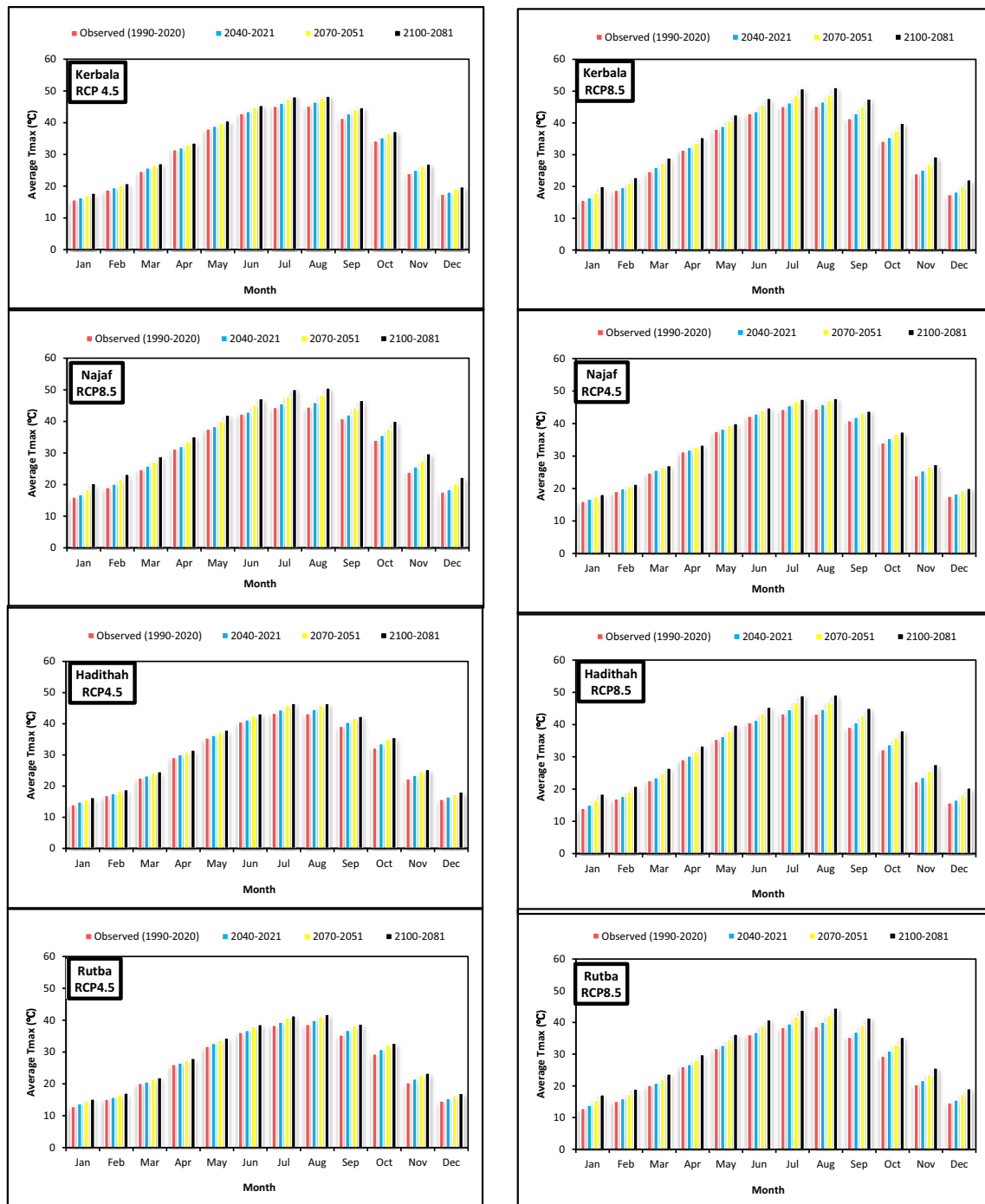
Fig. 4 Comparison average monthly temperatures of observed (1990–2020) with values forecast by using five GCMs models under scenarios RCP4.5 and RCP8.5 for three periods (2021–2040, 2051–2070, 2081–2100)

These rises in temperatures are expected to accelerate desertification [75], impacting agriculture [52], land use, land cover changes, and water supplies in Iraq. Increased surface water evaporation promotes water shortages, highlighting the need for sustainable solutions to reduce and adjust to these consequences. According to studies conducted in Iraq and around the world by researchers [76, 77], climate variations are a significant factor in the growth of sand and dust storms and other extreme weather events, which the regions in Iraq suffered from during recent periods.
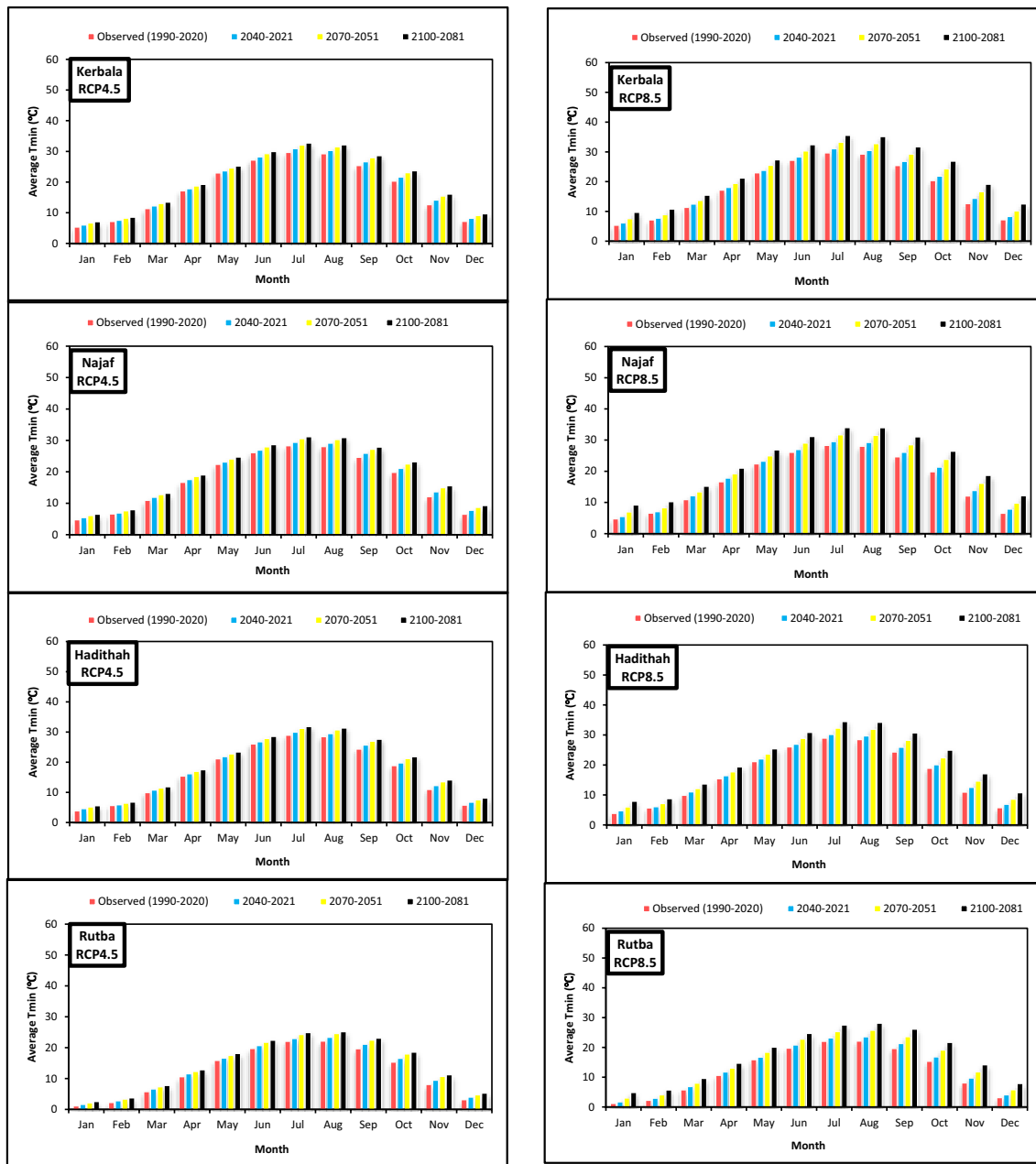
Fig. 4 (continued)

For the precipitation, the study revealed that the annual precipitation increase over the observed period is variable across periods and scenarios (RCP4.5 and RCP8.5), ranging from +6.09 to +14.31% and +11.25 to +20.97%, respectively. These results of increasing the amount of annual rainfall are consistent with previous research by researchers [73]. Also, this increase may be due to extreme rainy events that may occur unevenly during the rainy seasons. The projected increase in the amount and intensity of future rain events raises risks to the infrastructure and its resilience and may lead to flooding in the drainage systems in the future. A study by researchers [78, 79] in Iraq examines the link between 500 hPa geopotential height patterns and surface cyclones. Results show that an upper trough over the eastern Mediterranean increases warm and moist air advection, leading to baroclinic instability, significant heavy precipitation, and floods. According to the study, these aberrant atmospheric shifts might lead to the formation of extreme weather across the study region throughout the study time. The increase in rainfall in the rainy months for the study area can be beneficial to compensate for drought and water shortages in the summer
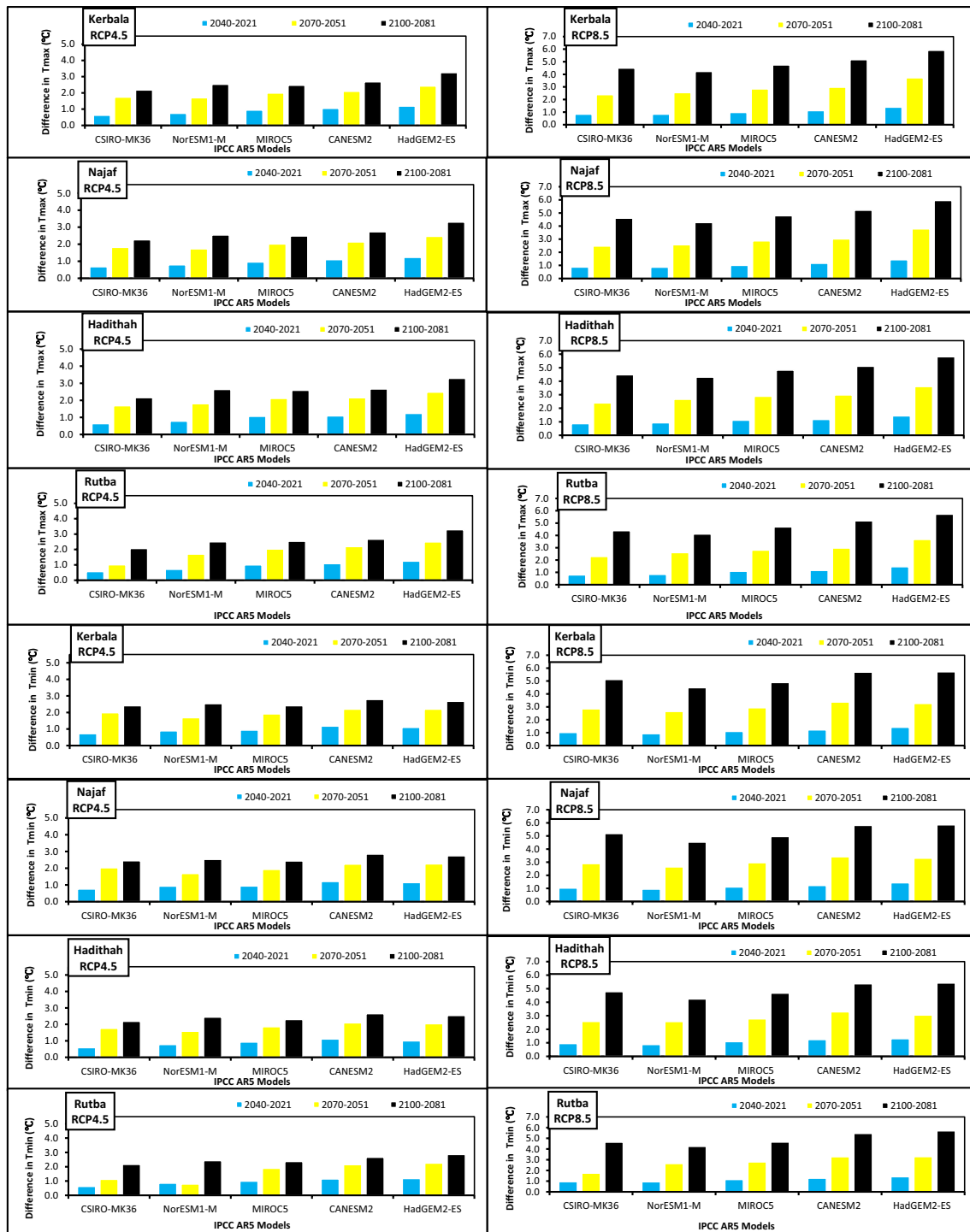
Fig. 5 Annual temperatures differences between three periods (2021–2040, 2051–2070, 2081–2100) and observed period (1990–2020)

months and be invested well and reasonably for agriculture, rainwater harvesting techniques, and others.

Although the phenomenon of climate change is a physical process linked to changes in climatic variables, it is also influenced by economic, environmental, and social processes involved in how civilization evolves over time. Mitigation and adaptation to climate change effects are based on proactive steps taken by socioeconomic groups in the study area. Techniques for climate change adaptation and mitigation include various fields, such as water management strategy, including long-term integrated national water resource
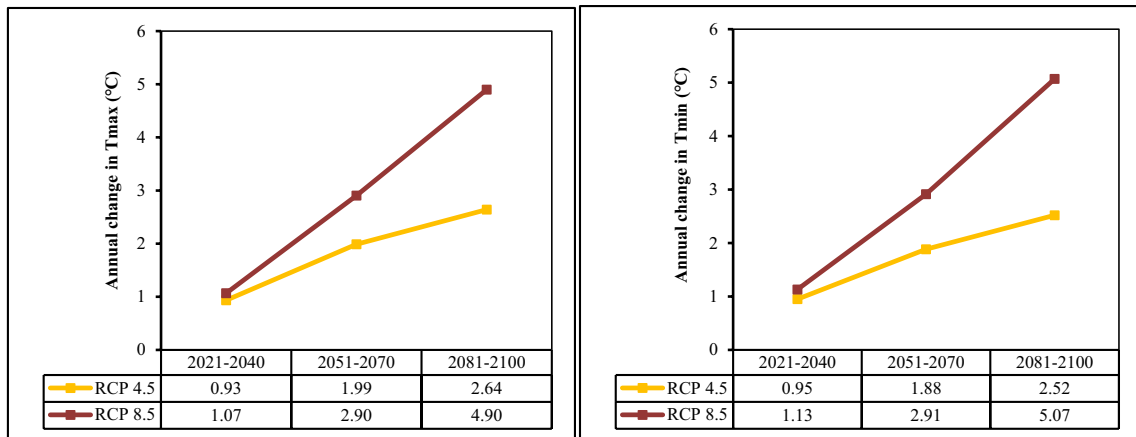
Fig. 6 Changes in predicted annual maximum and minimum temperatures in the future for average of the four selected stations
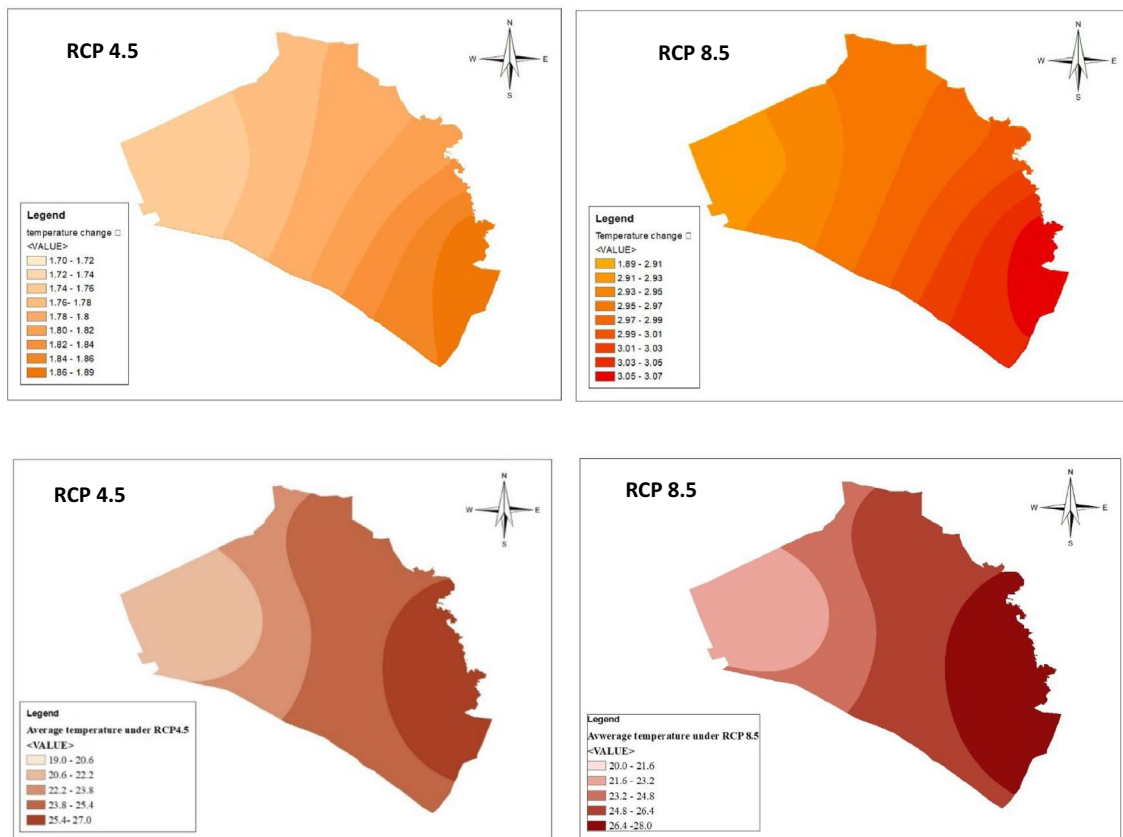
Fig. 7 a) Spatial distribution of the projected average temperature changes (°C) based on the baseline historical data (1990–2020), and b) projected average temperatures under RCP 4.5 and RCP 8.5 scenarios for future periods (2021–2100)

management and planning, rehabilitation of water treatment plant infrastructure, and the use of alternative water resources such as recycled waste water by establishing recycling water plants as well as water harvesting. Renewable energy investment opportunities and green infrastructure strategies, including solar and wind energy instead of fossil fuels, are needed to reduce greenhouse gas emissions and improve the environment.
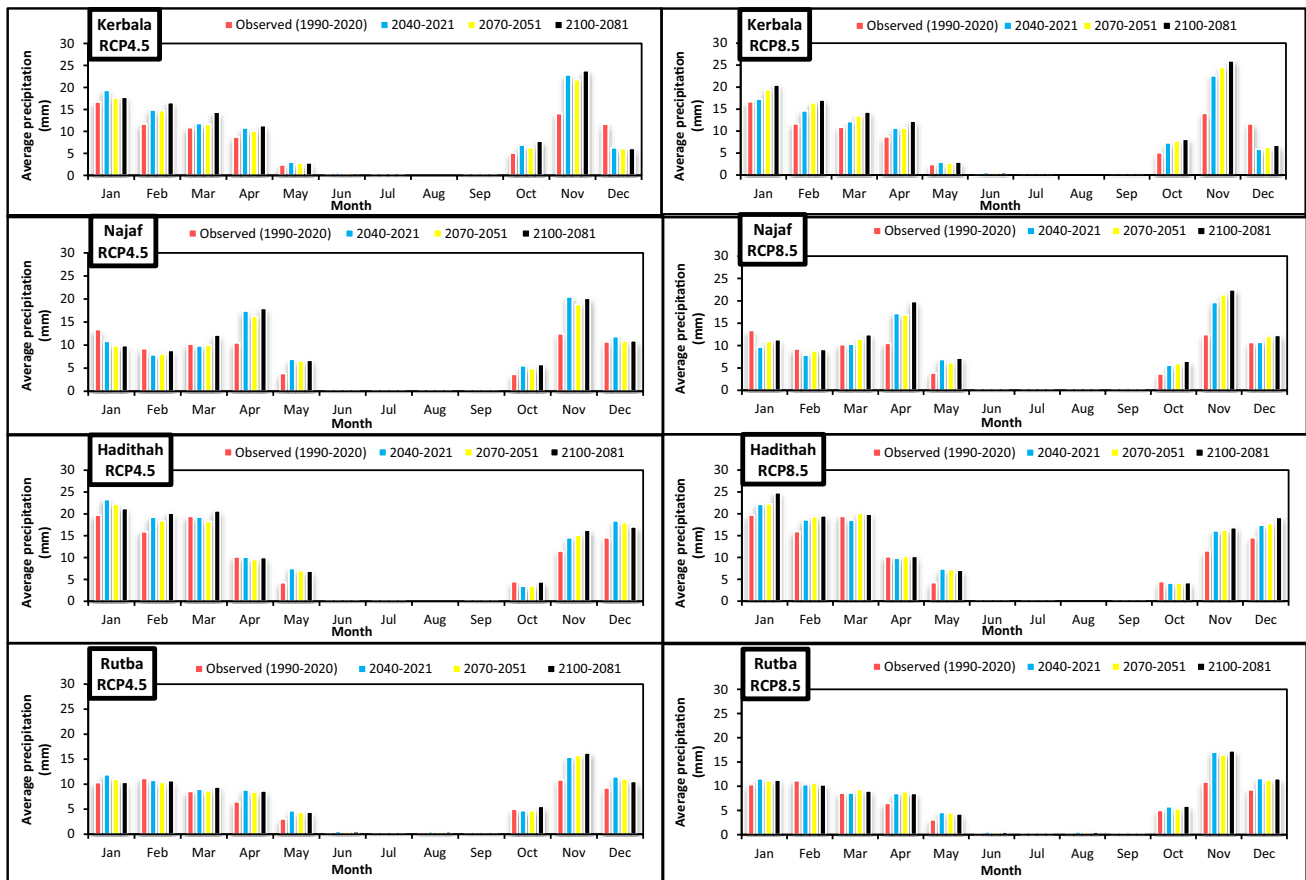
Fig. 8 Comparison average monthly precipitation of observed (1990–2020) with values forecast by using five GCMs models under scenarios RCP4.5 and RCP8.5 for three periods (2021–2040, 2051–2070, 2081–2100)

5 Conclusions

Climate change, especially rising temperatures in arid and semi-arid regions, is one of the most critical environmental challenges in human society, with several studies devoted to it in recent years. This study is essential for recognizing and evaluating the effects of climate change on the daily maximum temperatures, minimum temperatures, and precipitation for the middle and west regions of Iraq during the twenty-first century, divided into three future periods: the near future (2021–2040), medium future (2051–2070), and far future (2081–2100). Five GCM models (HadGEM2-ES, NorESM1-M, CanESM2, CSIRO-MK3.6.0, and MIROC5 models) under IPCC (AR5) scenarios (RCP4.5 and RCP8.5) are downscaled by using the LARS-WG model, which has been employed for this purpose. Based on the baseline data of 30 years from 1990 to 2020, it was used for the purpose of calibration and validation of the ability of the model to downscale and generate climate changes in the future for the four selected stations (Kerbala, Najaf, Hadithah, and Rutba) that represent the study area in the west and middle of

Iraq. The outcomes of this study showed that the LARS-WG model performed well for downscaling daily temperatures and precipitation. The results of the calibration process show that the model was skilled enough to simulate future climatic data. And statistical indicators R2, RMSE, and MBE showed a good correlation between the observed and generated data. Thus, increased confidence in the results of current research and the possibility of using the model in future applications. Compared to the baseline period, the LARS-WG model predicted a steady increase in temperature during the current century and reached its peak in the far future (2081–2100). Under both scenarios, RCP4.5 and RCP8.5, it is expected that the minimum and maximum annual temperatures will rise at all selected stations across future periods by an average of 0.94 and 4.98 °C. The HadGEM2-ES GCM model predicted a higher temperature rise for both scenarios than other models. The future predictions obtained by this study show a more extreme climate. Where it shows dry weather and high and increasing temperatures until the end of the twenty-first century. As a result, it may cause risks such as damage to the
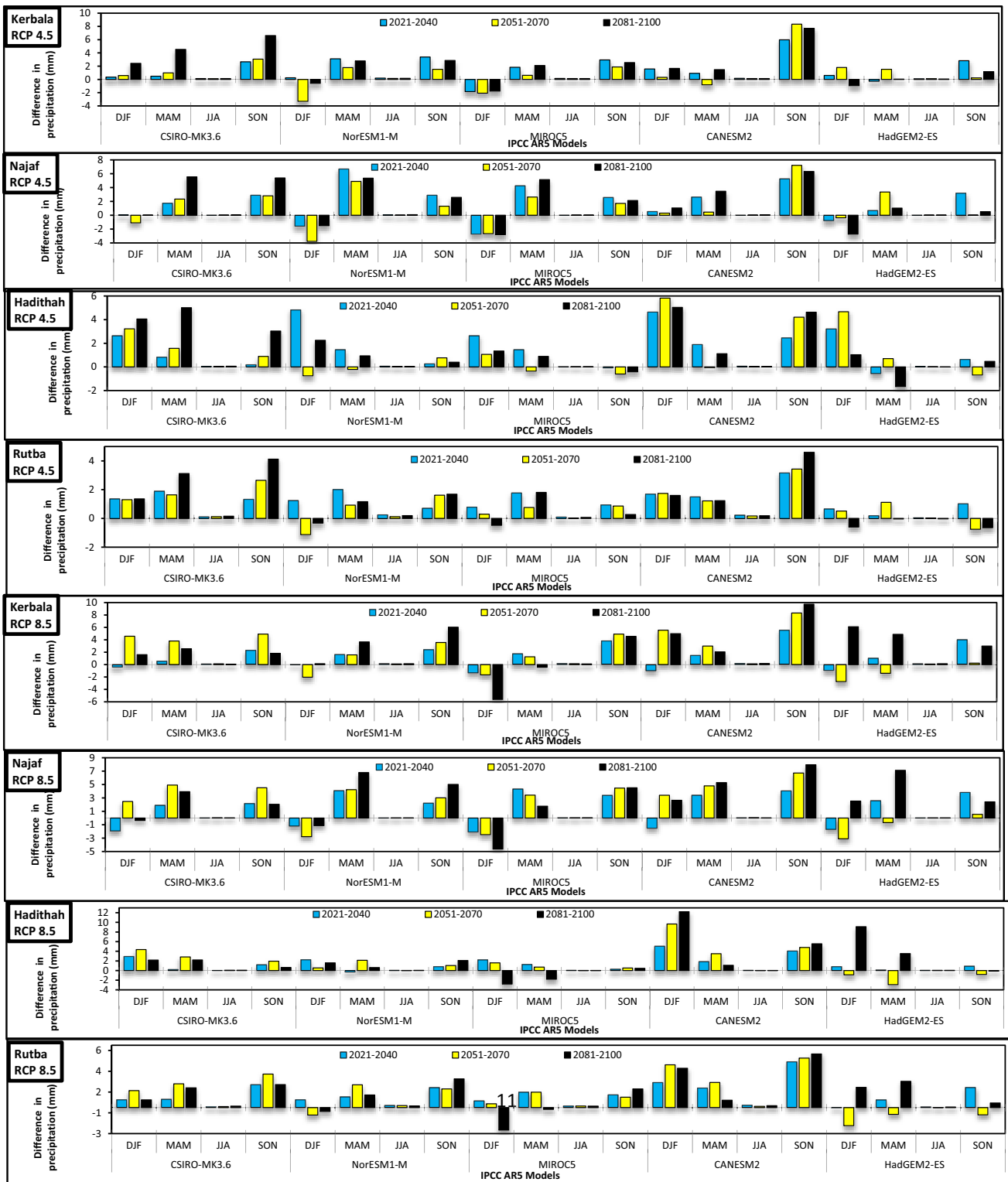
Fig. 9   Seasonal Precipitation differences between future and observed periods

production of agricultural crops, an increase in dust storms in the summer months, and drought. Keep in mind that a large percentage of the study area is desert.

And the study shows that the amount of rain during the rainy months in the study area will increase and vary according to each of the five selected models. Rainfall
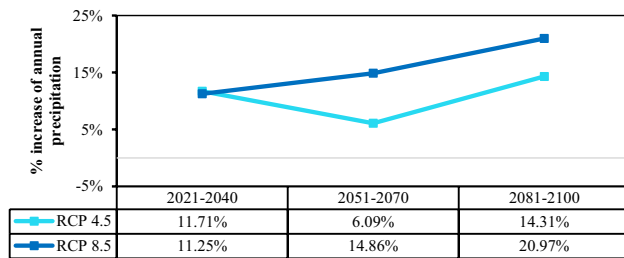
	2021-2040	2051-2070	2081-2100
RCP 4.5	11.71%	6.09%	14.31%
RCP 8.5	11.25%	14.86%	20.97%

Fig. 10 Percentage of average annual precipitation increases for four stations

increases during the rainy season can help compensate for droughts and summer water shortages and can be wisely invested for agriculture, rainwater gathering techniques, and other purposes. The results of this study will be useful to decision-makers in order to assist in developing the necessary plans to adapt to the effects of climate change in the region.

Declarations

References

1. Jason P (2008) 21st century climate change in the middle east. Clim Change. https://doi.org/10.1007/s10584-008-9438-5
2. Chen H et al (2013) Prediction of temperature and precipitation in Sudan and South Sudan by using LARS-WG in future. Theoret Appl Climatol 113:363–375. https://doi.org/10.1007/s00704-012-0793-9
3. Pachauri RK et al (2014) Climate change 2014: synthesis report. Contribution of Working Groups I, II and III to the fifth assessment report of the intergovernmental panel on climate change. Ipcc. https://epic.awi.de/id/eprint/37530/
4. Hassan WH, Nile BK, Al-Masody BA (2017) Climate change effect on storm drainage networks by storm water management model. Environ Eng Res 22(4):393–400. https://doi.org/10.4491/eer.2017.036
5. Stocker TF et al (2013) The physical science basis. Contribution of working group I to the fifth assessment report of the intergovernmental panel on climate change. Comput Geom 18(2):95–123
6. Mohammed MH, Zwain HM, Hassan WH (2021) Modeling the impacts of climate change and flooding on sanitary sewage system using SWMM simulation: a case study. Results Eng 12:100307. https://doi.org/10.1016/j.rineng.2021.100307
7. Norby RJ, Luo Y (2004) Evaluating ecosystem responses to rising atmospheric CO_2 and global warming in a multi-factor world. New Phytol 162(2):281–293. https://doi.org/10.1111/j.1469-8137.2004.01047.x
8. Mohsen KA, Nile BK, Hassan WH (2020) Experimental work on improving the efficiency of storm networks using a new galley design filter bucket. In: IOP conference series: materials science and engineering. IOP Publishing. https://doi.org/10.1088/1757-899X/671/1/012094/meta
9. Hassan WH et al (2021) A feasibility assessment of potential artificial recharge for increasing agricultural areas in the Kerbala desert in Iraq using numerical groundwater modeling. Water 13(22):3167. https://doi.org/10.3390/w13223167
10. Cubasch U et al (2001) Projections of future climate change, in Climate Change 2001: the scientific basis. Contribution of WG1 to the Third Assessment Report of the IPCC (TAR). Cambridge University Press, pp 525–582. https://pure.mpg.de/rest/items/item_1765171/component/file_1765201/content
11. Eden JM, Widmann M (2014) Downscaling of GCM-simulated precipitation using model output statistics. J Clim 27(1):312–324. https://doi.org/10.1175/JCLI-D-13-00063.1
12. Vanuytrecht E et al (2014) Comparing climate change impacts on cereals based on CMIP3 and EU-ENSEMBLES climate scenarios. Agric For Meteorol 195:12–23. https://doi.org/10.1016/j.agrformet.2014.04.017
13. Hassan WH (2021) Climate change projections of maximum temperatures for southwest Iraq using statistical downscaling. Clim Res 83:187–200. https://doi.org/10.3354/cr01647
14. Wilby RL et al (2009) A review of climate risk information for adaptation and development planning. Int J Climatol J R Meteorol Soc 29(9):1193–1215. https://doi.org/10.1002/joc.1839
15. Hassan WH, Khalaf RM (2020) Optimum groundwater use management models by genetic algorithms in Karbala Desert, Iraq. In: IOP conference series: materials science and engineering. IOP Publishing. https://doi.org/10.1088/1757-899X/928/2/022141/meta
16. Khaliq M (2019) An inventory of methods for estimating climate change-informed design water levels for floodplain mapping. Technical report
17. Mohammed MH, Zwain HM, Hassan WH (2022) Modeling the quality of sewage during the leaking of stormwater surface

runoff to the sanitary sewer system using SWMM: a case study. AQUA Water Infrastruct Ecosyst Soc 71(1):86–99. https://doi.org/10.2166/aqua.2021.227

18. Jalal HK, Hassan WH (2020) Three-dimensional numerical simulation of local scour around circular bridge pier using flow-3D software. In: IOP conference series: materials science and engineering. IOP Publishing. https://doi.org/10.1088/1757-899X/745/1/012150/meta

19. Xu Z, Han Y, Yang Z (2019) Dynamical downscaling of regional climate: a review of methods and limitations. Sci China Earth Sci 62:365–375. https://doi.org/10.1007/s11430-018-9261-5

20. Eum H-I, Gupta A, Dibike Y (2020) Effects of univariate and multivariate statistical downscaling methods on climatic and hydrologic indicators for Alberta, Canada. J Hydrol 588:125065. https://doi.org/10.1016/j.jhydrol.2020.125065

21. Lee C-Y et al (2020) Statistical–dynamical downscaling projections of tropical cyclone activity in a warming climate: two diverging genesis scenarios. J Clim 33(11):4815–4834. https://doi.org/10.1175/JCLI-D-19-0452.1

22. Hassan WH, Attea ZH, Mohammed SS (2020) Optimum layout design of sewer networks by hybrid genetic algorithm. J Appl Water Eng Res 8(2):108–124. https://doi.org/10.1080/23249676.2020.1761897

23. Adachi S, Tomita H (2020) Methodology of the constraint condition in dynamical downscaling for regional climate evaluation: a review. J Geophys Res Atmos 125(11):e2019JD032166. https://doi.org/10.1029/2019JD032166

24. Hassan WH et al (2023) Effect of artificial (pond) recharge on the salinity and groundwater level in Al-Dibdibba Aquifer in Iraq using treated wastewater. Water 15(4):695. https://doi.org/10.3390/w15040695

25. Rasheed AM (2018) Adaptation of water sensitive urban design to climate change. Queensland University of Technology, Brisbane. https://doi.org/10.5204/thesis.eprints.122960

26. Hassan WH et al (2022) Evaluation of gene expression programming and artificial neural networks in PyTorch for the prediction of local scour depth around a bridge pier. Results Eng 13:100353. https://doi.org/10.1016/j.rineng.2022.100353

27. Hashmi MZ, Shamseldin AY, Melville BW (2011) Comparison of SDSM and LARS-WG for simulation and downscaling of extreme precipitation events in a watershed. Stoch Env Res Risk Assess 25:475–484. https://doi.org/10.1007/s00477-010-0416-x

28. Semenov MA, Barrow EM, Lars-Wg A (2002) A stochastic weather generator for use in climate impact studies. User Man Herts UK, pp 1–27. http://resources.rothamsted.ac.uk/sites/default/files/groups/mas-models/download/LARS-WG-Manual.pdf

29. Wilby RL, Dawson CW (2004) Using SDSM version 3.1—a decision support tool for the assessment of regional climate change impacts. User Man 8:1–7

30. Zubaidi SL et al (2019) Using LARS-WG model for prediction of temperature in Columbia City, USA. In: IOP conference series: materials science and engineering. IOP Publishing. https://doi.org/10.1088/1757-899X/584/1/012026/meta

31. Costa-Cabral M et al (2013) Climate variability and change in mountain environments: some implications for water resources and water quality in the Sierra Nevada (USA). Clim Change 116:1–14. https://doi.org/10.1007/s10584-012-0630-2

32. Birara H, Pandey R, Mishra SK (2020) Projections of future rainfall and temperature using statistical downscaling techniques in Tana Basin, Ethiopia. Sustain Water Resour Manag 6:1–17. https://doi.org/10.1007/s40899-020-00436-1

33. Hassan I et al (2020) Selection of CMIP5 GCM ensemble for the projection of spatio-temporal changes in precipitation and temperature over the Niger Delta, Nigeria. Water 12(2):385. https://doi.org/10.3390/w12020385

34. Chisanga CB, Phiri E, Chinene V (2020) Reliability of rain-fed maize yield simulation using LARS-WG derived CMIP5 climate data at Mount Makulu, Zambia. J Agric Sci 12(11):275. https://doi.org/10.5539/jas.v12n11p275

35. Hailesilassie WT et al (2022) Future precipitation changes in the Central Ethiopian Main Rift under CMIP5 GCMs. J Water Clim Change 13(4):1830–1841. https://doi.org/10.2166/wcc.2022.440

36. Saddique N et al (2019) Downscaling of CMIP5 models output by using statistical models in a data scarce mountain environment (Mangla Dam Watershed), Northern Pakistan. Asia-Pac J Atmos Sci 55:719–735. https://doi.org/10.1007/s13143-019-00111-2

37. Punyawansiri S, Kwanyuen B (2020) Forecasting the future temperature using a downscaling method by LARS-WG stochastic weather generator at the local site of Phitsanulok Province, Thailand. Atmos Clim Sci 10(4):538–552. https://doi.org/10.4236/acs.2020.104028

38. Algretawee H et al (2022) Determination of difference amount in reference evapotranspiration between urban and suburban quarters in Karbala City. J Ecol Eng. https://doi.org/10.12911/22998993/149720

39. Fan X, Jiang L, Gou J (2021) Statistical downscaling and projection of future temperatures across the Loess Plateau, China. Weather Clim Extremes 32:100328. https://doi.org/10.1016/j.wace.2021.100328

40. Doulabian S et al (2021) Evaluating the effects of climate change on precipitation and temperature for Iran using RCP scenarios. J Water Clim Change 12(1):166–184. https://doi.org/10.2166/wcc.2020.114

41. Zakaria S, Al-Ansari N, Knutsson S (2013) Historical and future climatic change scenarios for temperature and rainfall for Iraq. J Civ Eng Archit 7(12):1574–1594

42. Yehia MA, Al-Taai OT, Ibrahim MK (2022) The chemical behaviour of greenhouse gases and its impact on climate change in Iraq. Egypt J Chem 65(131):1373–1382. https://doi.org/10.21608/ejchem.2022.151633.6571

43. Chen Z et al (2023) Satellite quantification of methane emissions and oil–gas methane intensities from individual countries in the Middle East and North Africa: implications for climate action. Atmos Chem Phys 23(10):5945–5967. https://doi.org/10.5194/acp-23-5945-2023

44. Hassan AS, Kadhum JH (2020) Assessment CO_2 emission intensity of crude oil production in Iraq. In: IOP conference series: materials science and engineering. IOP Publishing. https://doi.org/10.1088/1757-899X/928/7/072048/meta

45. Faruolo M et al (2022) A tailored approach for the global gas flaring investigation by means of daytime satellite imagery. Remote Sens 14(24):6319. https://doi.org/10.3390/rs14246319

46. Habeeb HB (2022) Assessing the contribution of tax revenues to overall economic growth expansion in the Iraqi economy during the course of the years 1990–2020. World Econ Finance Bull 15:95–103

47. Mohammed ZM, Hassan WH (2022) Climate change and the projection of future temperature and precipitation in southern Iraq using a LARS-WG model. Model Earth Syst Environ 8(3):4205–4218. https://doi.org/10.1007/s40808-022-01358-x

48. Khalaf RM et al (2022) Projections of precipitation and temperature in Southern Iraq using a LARS-WG stochastic weather generator. Phys Chem Earth Parts A/B/C 128:103224. https://doi.org/10.1016/j.pce.2022.103224

49. Hassan WH, Nile BK (2021) Climate change and predicting future temperature in Iraq using CanESM2 and HadCM3 modeling. Model Earth Syst Environ 7:737–748. https://doi.org/10.1007/s40808-020-01034-y

50. Hassan WH, Hashim FS (2020) The effect of climate change on the maximum temperature in Southwest Iraq using HadCM3

and CanESM2 modelling. SN Appl Sci 2(9):1494. https://doi.org/10.1007/s42452-020-03302-z

51. Saeed FH, Al-Khafaji MS, Al-Faraj FAM (2021) Sensitivity of irrigation water requirement to climate change in arid and semi-arid regions towards sustainable management of water resources. Sustainability 13(24):13608. https://doi.org/10.3390/su132413608

52. Osman Y, Al-Ansari N, Abdellatif M (2019) Climate change model as a decision support tool for water resources management in northern Iraq: a case study of Greater Zab River. J Water Clim Change 10(1):197–209. https://doi.org/10.2166/wcc.2017.083

53. Jalal HK, Hassan WH (2020) Effect of bridge pier shape on depth of scour. In: IOP conference series: materials science and engineering. IOP Publishing. https://doi.org/10.1088/1757-899X/671/1/012001/meta

54. Yuksel I (2015) South-eastern Anatolia Project (GAP) factor and energy management in Turkey. Energy Rep 1:151–155. https://doi.org/10.1016/j.egyr.2015.06.002

55. Hassan WH, Jalal HK (2021) Prediction of the depth of local scouring at a bridge pier using a gene expression programming method. SN Appl Sci 3(2):159. https://doi.org/10.1007/s42452-020-04124-9

56. Hassan WH et al (2022) Application of the coupled simulation–optimization method for the optimum cut-off design under a hydraulic structure. Water Resour Manag 36(12):4619–4636. https://doi.org/10.1007/s11269-022-03269-z

57. Fattah MY, Hassan WH, Rasheed SE (2018) Effect of geocell reinforcement above buried pipes on surface settlement. Int Rev Civ Eng 9(2):86–90

58. Abumoghli I (2015) Water scaurity in the Arab world. Ecomiddle East N Afr 2:2015

59. Kuylenstierna JL, Björklund G, Najlis P (1997) Sustainable water future with global implications: everyone's responsibility. In: Natural resources forum. Wiley Online Library. https://doi.org/10.1111/j.1477-8947.1997.tb00691.x

60. Al-Mussawi WH (2008) Kriging of groundwater level-a case study of Dibdiba Aquifer in area of Karballa-Najaf. J Kerbala Univ 6(1):170–182

61. Mueller A et al (2021) Climate change, water and future cooperation and development in the Euphrates-Tigris basin. ResearchGate/Geoscience/Report

62. Price R (2018) Environmental risks in Iraq. https://opendocs.ids.ac.uk/opendocs/handle/20.500.12413/13838

63. Adamo N et al (2018) Climate change: consequences on Iraq's environment. J Earth Sci Geotech Eng 8(3):43–58

64. Hassan WH, Hussein H, Nile BK (2022) The effect of climate change on groundwater recharge in unconfined aquifers in the western desert of Iraq. Groundw Sustain Dev 16:100700. https://doi.org/10.1016/j.gsd.2021.100700

65. Semenov MA, Barrow EM (1997) Use of a stochastic weather generator in the development of climate change scenarios. Clim Change 35(4):397–414. https://doi.org/10.1023/A:1005342632279

66. Semenov MA, Stratonovitch P (2010) Use of multi-model ensembles from global climate models for assessment of climate change impacts. Clim Res 41(1):1–14. https://doi.org/10.3354/cr00836

67. Semenov MA et al (1998) Comparison of the WGEN and LARS-WG stochastic weather generators for diverse climates. Clim Res 10(2):95–107

68. Pirttioja N et al (2015) Temperature and precipitation effects on wheat yield across a European transect: a crop model ensemble analysis using impact response surfaces. Clim Res 65:87–105. https://doi.org/10.3354/cr01322

69. Salman SA et al (2017) Long-term trends in daily temperature extremes in Iraq. Atmos Res 198:97–107. https://doi.org/10.1016/j.atmosres.2017.08.011

70. Salman SA et al (2018) Selection of climate models for projection of spatiotemporal changes in temperature of Iraq with uncertainties. Atmos Res 213:509–522. https://doi.org/10.1016/j.atmosres.2018.07.008

71. Hassan WH, Hashim FS (2021) Studying the impact of climate change on the average temperature using CanESM2 and HadCM3 modelling in Iraq. Int J Glob Warm 24(2):131–148. https://doi.org/10.1504/IJGW.2021.115898

72. Hassan WH (2020) Climate change impact on groundwater recharge of Umm er Radhuma unconfined aquifer Western Desert, Iraq. Int J Hydrol Sci Technol 10(4):392–412. https://doi.org/10.1504/IJHST.2020.108268

73. Eulewi HK (2021) The phenomenon of desertification in Iraq and its environmental impacts on middle and southern Iraq, Babil Governorate, as a model. In: IOP conference series: earth and environmental science. IOP Publishing. https://doi.org/10.1088/1755-1315/722/1/012020/meta

74. Faqe Ibrahim GR (2017) Urban land use land cover changes and their effect on land surface temperature: case study using Dohuk City in the Kurdistan Region of Iraq. Climate 5(1):13. https://doi.org/10.3390/cli5010013

75. Sissakian V, Al-Ansari N, Knutsson S (2013) Sand and dust storm events in Iraq. J Nat Sci 5(10):1084–1094. https://doi.org/10.4236/ns.2013.510133

76. Valavanidis A (2022) Extreme weather events exacerbated by the global impact of climate change. http://chem-tox-ecotox.org/wp-content/uploads/2023/02/EXTREME-WEATHER-EVENTS-CLIMATE-2022.pdf

77. Jabbar MAR, Hassan AS (2023) The daily pattern at 500 hPa geopotential heights and its association with heavy rainfall over Iraq. Iraqi J Sci. https://doi.org/10.24996/ijs.2023.64.3.38

78. Jabbar MAR, Hassan AS (2022) A cut-off low at 500 hPa geopotential height and rainfall events over Iraq: case studies. Iraqi J Phys 20(3):76–85. https://doi.org/10.30723/ijp.v22i3.1007

79. Adham A et al (2023) Rainwater catchment system reliability analysis for Al Abila Dam in Iraq's western desert. Water 15(5):944. https://doi.org/10.3390/w15050944